Co-robotic ultrasound tomography: dual arm setup and error analysis

Fereshteh Aalamifar[a], Dengrong Jiang[b], Haichong K. Zhang[c], Alexis Cheng[c], Xiaoyu Guo[a], Rishabh Khurana[d], Iulian Iordachita[d], Emad M. Boctor[a,c,e]

[a]Dept. of Electrical & Computer Eng., [b]Dept. of Biomedical Eng., [c]Dept. of Computer Science, [d]Dept. of Mechanical Eng., [e]Dept. of Radiology, Johns Hopkins University, Baltimore, MD, USA

ABSTRACT

Ultrasound (US) tomography enables quantitative measurement of acoustic properties. Robot assisted ultrasound tomography system enables alignment of two US probes. The alignment is done automatically by the robotic arm so that tomographic reconstruction of more anatomies becomes possible. In this study, we propose a new system setup for robot assistance in US tomographic imaging. This setup includes two robotic arms holding two US probes. One of the robotic arms is operated by the sonographer to determine the desired location for the tomographic imaging; this probe can also provide the B-mode US image during the search. The other robotic arm can then move automatically to align the two probes. One of the probes will act as transmitter and the other one as receiver to enable tomographic imaging. We provide an overview of the system setup and components together with the calibration procedures. In an attempt to provide a complete framework for the tomography system, we also provide a sample tomographic reconstruction method that can reconstruct speed of sound image using two aligned linear US probes. The reconstruction algorithm is however very prone to alignment inaccuracies. We provide an error propagation analysis to provide an estimation of the overall alignment error and then show the effect of the in-plane translational error in the tomographic reconstruction.

1. INTRODUCTION

Most clinically available US systems provide reflection US image and its varieties; however, reflection US imaging may miss some of the useful information that can be measured by tomographic US imaging [1]. In US tomographic imaging [1-10], the transmitter and receiver transducers are located at different known positions with respect to insonified volume and the received signal can be used to reconstruct the volume's acoustic properties such as speed of sound and attenuation. Previous attempts to allow US tomography has shown to be effective in breast cancer detection and diagnosis [1-6]. Duric *et al.* [1] used a circular array of US transducers in which at each time, one element transmits and others receive; this process is then repeated with a different element transmitting sequentially. Given that the geometry of the circular array of transducers is known, the radiological paths [11] can be reconstructed. This geometrical information, together with the received signal properties, such as time of flight and amplitude, are used to reconstruct tissue acoustic properties.

Another setup for tomographic US was investigated by several other groups [7-9]. Since an US probe, consists of an array of US transducers, two of such probes can be aligned along their axial axes to produce tomographic images. Aligning two probes manually is a challenging task. Hence we previously proposed robot assisted US tomography for tomographic US imaging using two conventional US probes, one operated by the sonographer as freehand and the other one moved by a robotic arm which keeps aligned with the freehand probe [12]. Such system could also facilitate tomographic reconstruction for more general examinations.

In this paper, we propose a new system setup for robot assistance in US tomographic imaging. Compared to our previous setup, the dual arm system does not require line of sight for tracking, it has the potential to be used as a fully robotic system or in a cooperative mode, and provides the operator with the option to fix the cooperative probe for tomographic imaging after the area of interest is found.

In the robot assisted US tomography system, one of the robotic arms is controlled by the sonographer. Then the other robotic arm can align the second US probe automatically. To enable such alignment, accurate calibrations between the two probes should be performed beforehand. Once the two probes are aligned, the US waves can be transmitted by one probe and received by the second one to allow for tomographic image reconstruction.

In this paper, we describe an algorithm for reconstructing speed of sound in US tomographic images using two aligned linear probes; the method is however very prone to positioning inaccuracies. We provide an analysis on how the tracking error propagates through the whole system and how the in-plane translational error affects the tomographic reconstruction.

Medical Imaging 2015: Ultrasonic Imaging and Tomography, edited by Johan G. Bosch, Neb Duric, Proc. of SPIE Vol. 9419, 94190N · © 2015 SPIE
CCC code: 1605-7422/15/$18 · doi: 10.1117/12.2084529

2. SYSTEM OVERVIEW

The dual arm system setup, shown in Fig. 1, consists of two robotic arms, and two US probes. Each of the arms can be controlled by the technician while the other one automatically aligns with it. To calculate the desired pose of the second arm, several calibrations are required. In this section, we explain the system components, then describe the calibrations in the next section.

Robotic arms

We used two 6 degrees of freedom UR5 robotic arms (Universal Robots, Odense, Denmark) which have 850 mm in radius spherical reach, and 0.1 mm repeatability. UR5 is a rather small robotic arm with 149 mm in diameter circular base and 75 mm in diameter circular tooltip; it is also a lightweight robotic arm (18.4 kg) and can be mounted on a portable cart. We have designed and manufactured a portable dual arm cart, as shown in Fig. 1(a), where the two robotic arms can be installed. There is a space on the lower part of the cart to put the robot controllers.

US probes

Two identical 60 mm 128 array linear Ultrasonix US probes, together with the Sonix Touch US machine (Analogic Ultrasound, Richmond, BC, Canada), were used. We designed and manufactured US probe holders that enable the attachment of the US probe to the robot tooltip. Fig. 1(b) shows the designed holder from different views. The holders were 3D printed using ABS material. It should be noted that, detaching and attaching the probe holders in a different orientation invalidates the calibrations. Hence, the probe holders have some markers to make the attachment reproducible as much as possible. However, even untightening the holders' screws may easily degrade the calibration accuracies in a millimeter range.

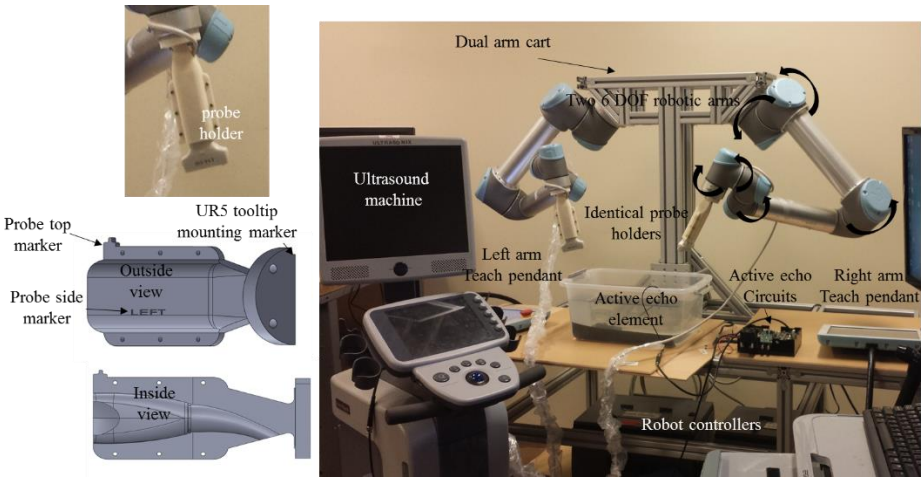

(b) (a)

Figure 1. Dual robotic arm US tomography system setup for calibrations. (a) System components; Robot's degrees of freedom are shown using black arrows. (b) Probe holders and the designed markers to maintain attachment's repeatability.

3. CALIBRATIONS

As mentioned before, one of the robotic arms will be controlled by the technician. To calculate the desired pose of the other arm, such that the two probes are aligned, the following equation can be used (Fig. 2):

$$B_2' = X_3^{-1} B_1 X_1 D X_2^{-1} \quad (1)$$

where B_2' is the desired pose for the second arm, B_1 is the first arm's pose, and D is the desired transformation from first US probe image frame to the second.

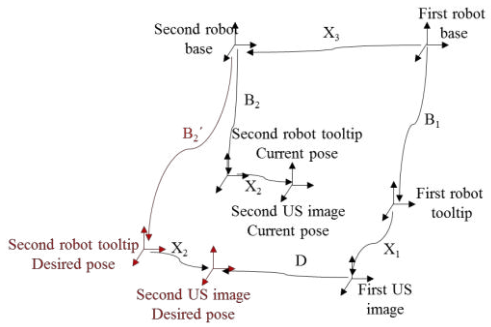

Figure 2. Transformations involved in calculating the desired second arm pose such that the two US probes are aligned.

B_1 and B_2 can be read from robot encoders; however, X_1, X_2, and X_3 should be determined through calibrations. X_1 and X_2 are the transformation matrices from robot tooltips to US images and hence are called US calibrations. X_3 is the transformation between the two robotic arm bases.

US calibrations

To find X_1 and X_2, we used an active echo US calibration [13] (the active echo circuitry is shown in Fig. 1 (a)). This is a point based calibration in which the active echo is imaged by the US probe from various poses. Active echo is an active miniaturized US element that listens to US signals. It sends back an US signal when it receives one. When the US probes trigger signals are connected to the active echo circuitry, it can measure the delay between the time US signal was transmitted by US probe and the time it was received by the active echo element. In addition, the probe's element with minimum delay can be determined. These two parameters can be used to localize the active echo element in US image coordinate frame.

To have an accurate US calibration, we always need to ensure active echo is in the US image mid-plane. Hence, we moved the robotic arm to various poses, and at each pose, stored two readings: 1. Robot tooltip frame position and orientation in robot base frame. 2. 2-D location of the active echo in US image frame.

We collected 28 data points for each arm and used the gradient descent algorithm [14] to solve for X_1 and X_2. To evaluate the calibrations, for each arm, we collected another data set, called test set, containing 9 data points. We consider the standard deviation of the reconstructed test points in robot base frame as a representation of the calibrations' precision. The calculated reconstruction precisions are [1.47, 0.51, 0.22] and [1.66, 0.69, 0.91] mm for the left and right arms respectively (Fig. 1).

Calibration of robot bases

We used the calculated X_1 and X_2 to calibrate the robot bases, i.e., find X_3. We moved the active echo point to 15 different poses (not in a line), and at each pose, we aligned the US images using the two arms (one by one) with the active echo, and collected data. These points can then be reconstructed in the two robot bases (using $P_j^i = B_j^i X_j p_j^i$, $j = \{1,2\}, i = \{1:15\}$ where P_j^i is point i defined in robot base j, B_j^i is the ith pose of jth robot tooltip in its base coordinate frame, and p_j^i is the location of ith active echo in jth US image). Hence, we have 15 points defined in the two coordinate frames. We used point cloud to point cloud registration (with known correspondences) to solve for X_3. We also collected a test set to evaluate the calibration precision. We fixed the active echo at 5 different poses, then scanned it using the two arms, but this time, reconstructed the points in the first robot base ($P_1^k = B_1^k X_1 p_1^k$, $P_2^k = X_3 B_2^k X_2 p_2^k$, $k = \{1:5\}$). The mean distance between the reconstructed points were considered as a representation of precision and was calculated as [3.30, 0.58, 1.67] mm.

4. ALIGNMENT USER INTERFACE

We developed a graphical user interface in Matlab, to control the arms and enable automatic alignment. Fig. 3 shows a screenshot of the designed user interface. Video 1 also shows a sample control of the two robotic arms. The user interface consists of several sections:

1. Connections: this part establishes an Ethernet connection between the user interface and robot control panel. A script on the robot control panel is written which can create a TCP/IP connection; send robot poses when requested; receive robot poses, and move the tooltip to the desired robot pose. The input to this section is the two controllers' IP addresses.
2. Cooperating arm: in this part, the user can determine which arm, he/she wants to control. The other arm will automatically align the two probes if the Align box is checked.
3. UR5 Control Panel: this section of the interface simulates the UR5 control panel. The user can control the cooperating arm, in all the six degrees of freedom, and in US image axes, using the buttons in this section.
4. After the movement is done, the control/ display area, on the right side of the interface, can be used to save robot poses and display the transformation between the US images' frames.

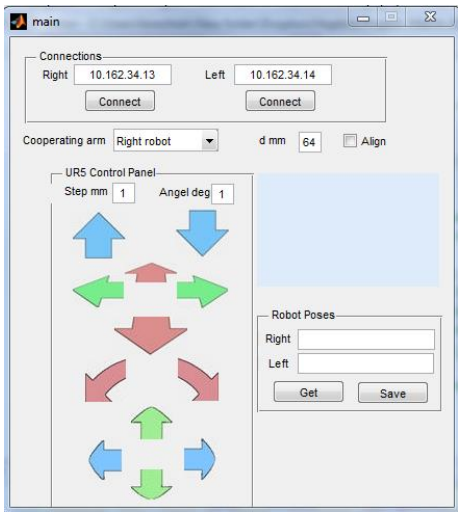

Figure 3. A screenshot of the alignment user interface

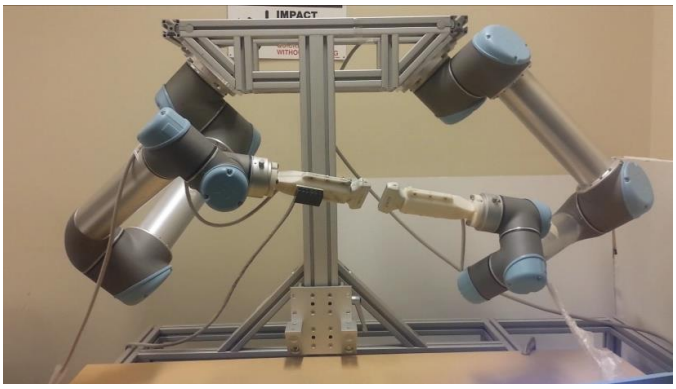

Video 1. A sample demonstration of using user interface to control and align the US probes. http://dx.doi.org/10.1117/12.2084529.1

5. TOMOGRAPHIC RECONSTRUCTION

In this section, we provide an algorithm for reconstructing speed of sound in the insonified area between two aligned linear arrays of US transmitters and receivers. The algorithm is based on one shot of transmitting and receiving between two aligned US probes when they are fixed in front of each other. Each probe contains an array of linearly positioned US transducer capable of both transmitting and receiving. One probe is selected as transmitter and the other one as receiver. The elements on the transmitting probe fire sequentially and send a trigger signal at the beginning of transmission. This trigger signal can be connected to the receiving probe to start collecting data. We assume that the US signal transmitted by each element can be received by all elements of the receiving probe.

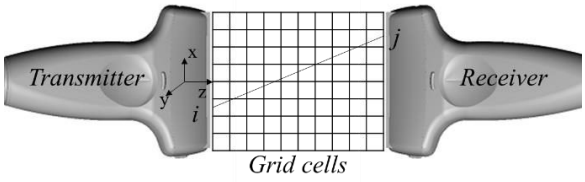

Figure 4. The insonified area divided into grid cells and one example transmit-receive ray from *i*th transmitter to the *j*th receiver. Also the Image axes directions is shown for transmitter.

System matrix

System matrix, S, contains the geometrical relation between transmitters and receivers. The insonified area can be divided into grid cells. The transmitters fire sequentially, and at each transmit firing, all the receivers are listening. The signal travels from one transmitter to all the receivers as shown in Fig. 4. There is a ray between each transmit receiver pair that passes through several grid cells.

The system matrix determines how much of each grid cell is passed by each ray. This matrix has $N_t \times N_r$ rows and N_g columns, where N_t is the number of transmitting elements, N_r is the number of receiving elements, and N_g is the total number of grid cells. Each row of the system matrix, corresponds to one pair of transmitter-receiver, and contains the path lengths corresponding to each grid cell. We constructed system matrix based on the method presented in [11] and using US probe lateral size, number of element in one probe, and the distance between the two probes. We ignored the elements' width or height and assumed the location of each transmitter/receiver is in the center. We also neglected bending of rays due to refraction and assumed the US signal travels along a straight line.

Time of flight

Time of flight, tof, is a vector that contains the time it took the signal to travel from a transmitter to a receiver. This vector has $N_t \times N_r$ number of rows, where each row corresponds to one ray, i.e. one transmit-receive pair.

Speed of sound

Our goal is to estimate the speed of sound in each cell of the grid, $v_i, i = \{1: N_g\}$. Instead of directly calculating v_i, we calculate its inverse, b_i, which is called "slowness". The time required for an ultrasound signal to travel along a ray is equal to the sum of the time through all cells it passes through; and the time required to travel through one cell is $t = l * b$, where l is the path length along the cell, and b is the cell's slowness. Hence, $tof_j = \sum_{i=1}^{n} S_{i,j} * b_i$, where tof_j is the total time of flight for the jth ray, $S_{i,j}$ is the path length of jth ray along ith cell and b_i is the ith cell slowness. This leads to solving the following equation for b:

$$S * b = tof \quad (2)$$

where b is the slowness vector with N_g number of rows.

The number of unknowns is N_g and the number of equations is $N_t \times N_r$. To solve this equation, one way is to use pseudoinverse, i.e.,

$$b = pinv(S) * tof \quad (3)$$

where $pinv()$ is the Moore-Penrose pseudoinverse. However, Duric *et al.* [3] found that, this equation, in practice, is difficult to solve; and more accurate results can be obtained if instead of absolute tof and b values (called Reconstructed in figures), their difference from a nominal value is measured (Diff-Reconstructed). In addition, to compensate for incomplete tomographic data and possible noise/error, we tested a total variation with conjugate gradient regularization algorithm [15] (TVCG and Diff-TVCG). We tested the tomographic reconstruction algorithm in simulation. A ground truth image was created by assigning speed of sound of 1540 m/s for background and 1490 m/s for a circular area with diameter 6 mm centered at [-5,0,12] mm in the image. The system matrix was reconstructed by considering 64 transmitting, and 64 receiving elements, each with 30 mm lateral length, and positioned at an axial distance of 30 mm (we assumed half of real probe dimensions for faster simulations). The transmitters and receivers are considered to have a neglecting width and are put side by side with 0.4688 mm distance from each other (deduced from the length of the probe and number of elements). The ground-truth image is shown in Fig. 5. The pixel intensities represent slowness for speed of sound range from 1450 to 1550 m/s. As shown in Fig 5, we first use the system matrix to produce the simulated time of flights, then calculate the speed of sound in grid cells using the absolute and differential pseudoinverse or regularized methods.

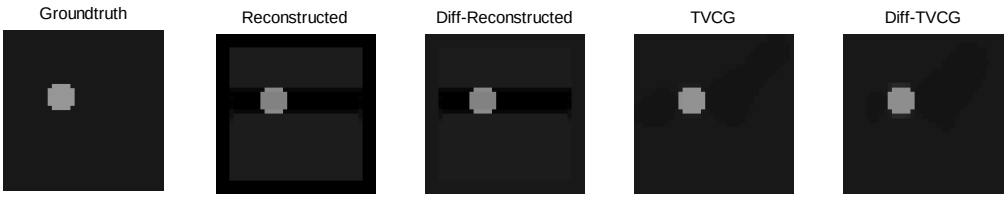

Figure 5. Ground-truth and reconstructed images without any inaccuracies or noise. The pixel intensities represent the slowness; the speed of sound is 1540 m/s in the background and 1490 in the circle of interest.

The reconstructed speed of sound in the absolute or difference methods are similar when no noise exists. However, the regularized images have a more uniform estimated speed of sound in the background but have shadows around the reconstructed circular area. These figures, however, show the reconstruction results when no noise or inaccuracy in the alignment exists. In the next section, we provide an error propagation analysis to find the range of expected alignment inaccuracy and then show the effect of in-plane translational error on the image reconstruction.

6. ERROR ANALYSIS

In this section, firstly, we investigate the effect of tracking inaccuracies in the overall alignment. In other words, we are interested in analyzing the resulting error in the transformation matrix, D, between the two US image frames. By looking at Fig. 2, D can be calculated using the following equation:

$$D = X_1^{-1} B_1^{-1} X_3 B_2 X_2 \quad (4)$$

The above equation holds when all the matrices are accurate. Considering inaccuracies, we have the following equation:

$$D\Delta D = \Delta X_1^{-1} X_1^{-1} \Delta B_1^{-1} B_1^{-1} X_3 \Delta X_3 B_2 \Delta B_2 X_2 \Delta X_2 \quad (5)$$

where ΔD is the measurement error in D; similarly other matrices have their own errors. By taking D to the right side we have the following equation:

$$\Delta D = D^{-1} \Delta X_1^{-1} X_1^{-1} \Delta B_1^{-1} B_1^{-1} X_3 \Delta X_3 B_2 \Delta B_2 X_2 \Delta X_2 \quad (6)$$

Here, we make the assumption that the desired D matrix is a rotation of 180 degrees about x-axis and a translation along z-axis. Because ideally, we want the two probes to be aligned in front of each other, i.e., second probe's frame origin be rotated 180 degrees about the first probe frame's x-axis; and have an offset along first probe frame's z-axis. We chose this translation randomly from [0,150] mm. We used the calibration matrices found for the dual arm setup and defined a random transformation matrix from first robot base to its tooltip, B_1. Then we calculate B_2 using equation (4).

Based on Rodrigues formula, every rigid-body rotation can be defined by a unit vector, ω, as the axis of rotation, and a magnitude of rotation angle, θ:

$$R = e^{\theta \hat{\omega}} = I + \sin(\theta)\, \hat{\omega} + (1 - \cos(\theta))\hat{\omega}^2 \quad (7)$$

where $\hat{\omega}$ is the skew-symmetric matrix made from ω. When θ is a small value (in case of rotation errors), the above formula can be written as:

$$R \approx I + \theta \hat{\omega} \quad (8)$$

We used this formula to define rotation errors. For B_1 and B_2, we considered a maximum rotation angle error of 1 degree (0.0175 radian) and a maximum translation error of 0.1 mm. Since the inaccuracy is not always at its maximum for the robot transformations, at each time, we picked the current rotation and translation errors from zero to maximum error randomly. However, the calibration matrices have a constant error and hence their error matrices were defined using a constant magnitude of translational and angular error. It should be noted that the translational error is the norm of the errors in the three axes. The axes of rotational and translational errors were also picked randomly. Now, all the matrices in the right hand side of equation (6) are defined or randomly selected, hence, ΔD can be calculated. We repeated this process 20 times for each error value for the calibration matrices' errors (we assumed same error for all the three calibrations), 20 randomly selected other matrices, and got the average resulting translational and rotational errors derived from ΔD. Fig. 6 shows the results.

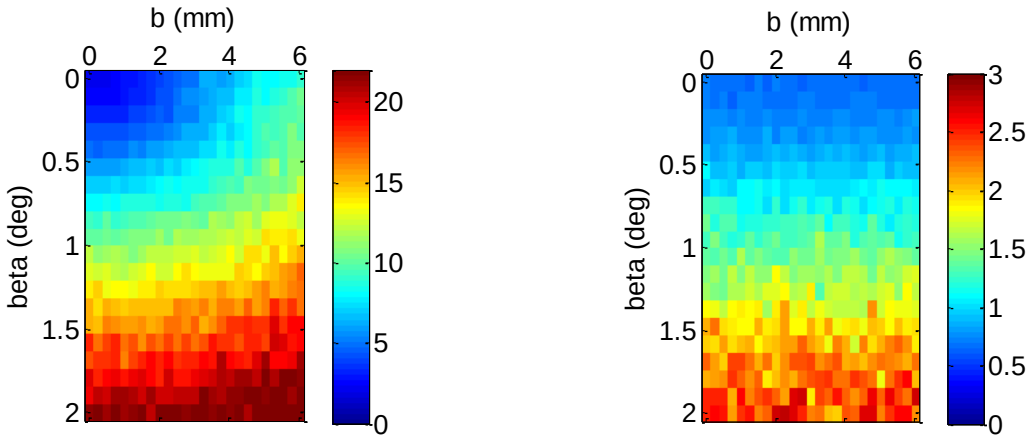

Figure 6. Error in the transformation between the probes as a function of calibrations error. (a) translational error (mm). (b) rotational error (degrees).

Focusing on the translation error, we can examine the error in each individual axis. Figure 7 shows the decomposed translational error in the three axes; the axes are defined as shown in Fig. 4.

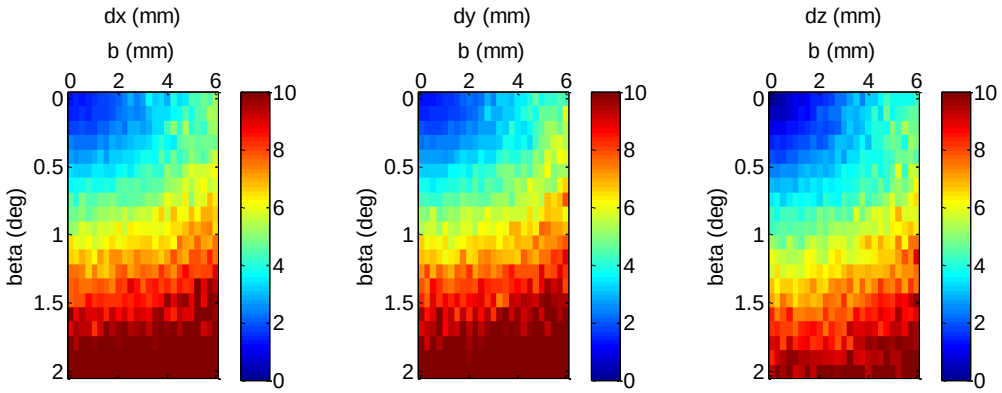

Figure 7. The translational error of the transformation between the two US image coordinate frames in individual axes; The axes are shown in Fig. 4.

The amount of the error is almost similar among the three axes (the axial error seems to be less than the other two axes). However, they might have different effects on the reconstruction. It is not easy to determine the error from calculated reconstruction precisions in the experimental setup; however, we can expect a translational error less than 4 mm; assuming the rotational error is less than 0.5 degrees, the expected error in each axis will be around 3 mm. Here, we only applied the in-plane translational error on the reconstruction algorithm. The effect of out-of-plane and rotational errors can be investigated similarly but requires the construction of system matrix in 3 dimensions. As shown in Fig. 8, the absolute algorithms are very sensitive to any alignment error. The difference algorithms, esp. Diff-TVR, is the most robust method. However, they require imaging of the background which might be difficult in a clinical setting.

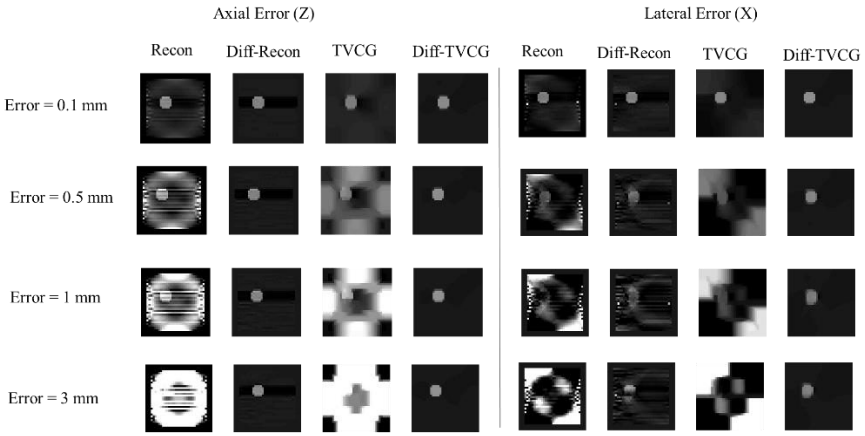

Figure 8. Effect of in-plane translational error on tomographic reconstruction for the expected range of errors.

7. CONCLUSIONS

US tomography can be used to measure acoustic properties quantitatively. In this paper, we proposed a dual robotic arm setup that can be used to align two US probes for US tomography. We provided the calibrations required to enable the alignment; then explained an algorithm that can reconstruct speed of sound when such two probes are aligned. We also provided an error analysis for the system. In the future, we are considering methods of correcting for alignment error using US signals. In this paper, we provided some sample reconstruction algorithm with an incomplete set of data, collected from one pose. Looking at more variety of reconstruction algorithms with extra data sets from more angles is another interesting area of research.

ACKNOWLEDGMENT

Financial support was provided by Johns Hopkins University internal funds and NSF grant IIS-1162095.

REFERENCES

[1] Duric, Nebojsa, Peter Littrup, Lou Poulo, Alex Babkin, Roman Pevzner, Earle Holsapple, Olsi Rama, and Carri Glide. "Detection of breast cancer with ultrasound tomography: First results with the Computed Ultrasound Risk Evaluation (CURE) prototype." Medical physics 34, no. 2 (2007): 773-785.
[2] Delphinus Medical Technologies, “http://www.delphinusmt.com/our-technology/softvue-system.” Accessed 1/11/2015.
[3] Duric, Nebojsa, Peter Littrup, Alex Babkin, David Chambers, Stephen Azevedo, Arkady Kalinin, Roman Pevzner, Mikhail Tokarev, and Earle Holsapple. "Development of ultrasound tomography for breast imaging: Technical assessment." Medical Physics 32.5 (2005): 1375-1386.
[4] Li, Cuiping, Nebojsa Duric, Peter Littrup, and Lianjie Huang. "In vivo Breast Sound-Speed Imaging with Ultrasound Tomography." Ultrasound in medicine & biology 35.10 (2009): 1615-1628.
[5] Glide, Carri, Nebojsa Duric, and Peter Littrup. "Novel approach to evaluating breast density utilizing ultrasound tomography." Medical physics 34.2 (2007): 744-753.
[6] Littrup, Peter J., Neb Duric, Stephen Azevedo, David Chambers, James V. Candy, Stephen Johnson, Gregory Auner, John Rather, and Earle T. Holsapple. "Computerized ultrasound risk evaluation (CURE) system: Development of combined transmission and reflection ultrasound with new reconstruction algorithms for breast imaging." Acoustical Imaging. Springer US, 2002. 175-182.
[7] Jago, J. R., and T. A. Whittingham. "Experimental studies in transmission ultrasound computed tomography." Physics in medicine and biology 36.11 (1991): 1515.
[8] Marmarelis, Vasilis Z., Tae-Seong Kim, and Ramez EN Shehada. "High-resolution ultrasound transmission tomography." Medical Imaging 2003. International Society for Optics and Photonics, 2003.

[9] Ashfaq, Mohammad. Measuring and Signal Processing Techniques for Ultrasound Computed Tomography. Diss. PhD thesis. Bochum, Germany: Ruhr University, 2007.
[10] Greenleaf, James F. "Computerized tomography with ultrasound." Proceedings of the IEEE 71.3 (1983): 330-337.
[11] R. L. Siddon. "Fast calculation of the exact radiological path for a three-dimensional CT array." Medical physics 12.2 (1985): 252-255.
[12] Aalamifar, Fereshteh, Rishabh Khurana, Alexis Cheng, Russell H. Taylor, Iulian Iordachita, and Emad M. Boctor. "Enabling technologies for robot assisted ultrasound tomography: system setup and calibration." SPIE Medical Imaging. International Society for Optics and Photonics, 2014.
[13] Guo, Xiaoyu, Alexis Cheng, Haichong K. Zhang, Hyun-Jae Kang, Ralph Etienne-Cummings, and Emad M. Boctor. "Active echo: a new paradigm for ultrasound calibration." Medical Image Computing and Computer Assisted Intervention 2014.
[14] Ackerman, Martin Kendal, Alexis Cheng, Emad Boctor, and Gregory Chirikjian. "Online ultrasound sensor calibration using gradient descent on the Euclidean Group." Robotics and Automation (ICRA), 2014 IEEE International Conference on. IEEE, 2014.
[15] M. Lusting, SparseMRI Toolbox downloaded from http://www.eecs.berkeley.edu/~mlustig/Software.html. Downloaded: 08/01/2014.